Computers and Chemical Engineering 134 (2020) 106686

Contents lists available at ScienceDirect

Computers and Chemical Engineering

journal homepage: www.elsevier.com/locate/compchemeng

# Multi-phase particle-in-cell coupled with population balance equation (MP-PIC-PBE) method for multiscale computational fluid dynamics simulation

Shin Hyuk Kim[a], Jay H. Lee[a,*], Richard D. Braatz[b]

[a] Department of Chemical and Biomolecular Engineering, Korea Advanced Institute of Science and Technology, 291 Daehak-Ro, Yuseong-Gu, Daejeon 34141, South Korea

[b] Massachusetts Institute of Technology, 77 Massachusetts Avenue, Cambridge, MA 02139, United States

ARTICLE INFO

*Article history:*
Received 16 August 2019
Revised 6 November 2019
Accepted 20 December 2019
Available online 23 December 2019

*Keywords:*
Multiphase particle in cell
Dense particulate flow
Population balance equation
Computational fluid dynamics
Multiscale simulation

ABSTRACT

The 'multiphase particle-in-cell coupled with population balance equation' (MP-PIC-PBE) method is introduced for simulating multi-scale multiphase particulate flows. This method couples the meso–scale fluid dynamics simulated by the MP-PIC method with the simulation of the micro-scale particle size distribution. The homogeneous population balance equation is calculated for each discrete particle tracked in a Lagrangian frame, after the MP-PIC numerical procedure is followed at each time instance. This approach allows the particulate phase to accommodate the particulate stresses using spatial gradients and allows the Lagrangian description to predict particle properties by the PBE. For the antisolvent crystallization of Lovastatin in a biradial mixer, the proposed method is compared to an existing method that simulates the spatiotemporal evolution of the particle distribution by combining a multi-environment probability density function with the spatially varying PBE. The MP-PIC-PBE method has lower computational cost and provides more detailed information, such as particle age and location.



## 1. Introduction

Several solvers are available for the simulation of multiphase particulate flow, which can be broadly categorized into Euler-Eulerian and Euler-Lagrangian approaches (Goldschmidt et al., 2004). The Euler-Eulerian approach expresses all phases using the continuum governing equations, with particle-particle stresses expressed using spatial gradients of the volume fraction and the velocity. The approach applies to flows of any particle density. A drawback of the approach is that modeling the flow of particles of different types and sizes complicates the continuum formulation because it requires a separate model for each type and size (Ding and Gidaspow, 1990; Khopkar et al., 2006).

The spatiotemporal evaluation of a distribution of particles in Euler-Eulerian methods can be modeled by using the population balance equation (PBE) (Xie and Luo, 2017). However, solving both the PBE and fluid dynamics equations simultaneously is costly because it involves a partial differential equation with at least five dependent variables: time, 3-dimensional space, and particle distribution variable (e.g., size) (Rigopoulos, 2010). The method of moments is an efficient alternative to reduce the computational cost of simulating a PBE, but provides much less information on the particle distribution (Marchisio and Fox, 2005; Marchisio et al., 2003).

The Euler-Lagrangian approach uses the Lagrangian description for the particulate phase and the Euler description for the continuum phase. Using this approach, the particles can have different sizes, shapes, densities, and velocities (Fernandes et al., 2018). However, when the volume fraction of particles in the system is greater than 5%, the frequency of particle collisions is unrealistically increased and accuracy is drastically lowered (O'Rourke, 1981). Based on the PIC method (Harlow and Amsden, 1971) developed since the 1960s, the MP-PIC method (Andrews and O'Rourke, 1996; Snider, 2001; Snider et al., 1998) computes the stresses of dense particles using interpolations between grids and discrete particles. PIC-based methods can accommodate flows involving chemical reactions (O'Rourke et al., 1993). However, the computational cost is high when expressing chemical reactions or mass transfer to all the particles represented by Lagrangian frames and simulating changes in particle distribution at the micro scale with the fluid dynamics in the same scale.

* Corresponding author.
*E-mail addresses:* kimshinhyuk@kaist.ac.kr (S.H. Kim), jayhlee@kaist.ac.kr (J.H. Lee), braatz@mit.edu (R.D. Braatz).

https://doi.org/10.1016/j.compchemeng.2019.106686
0098-1354/

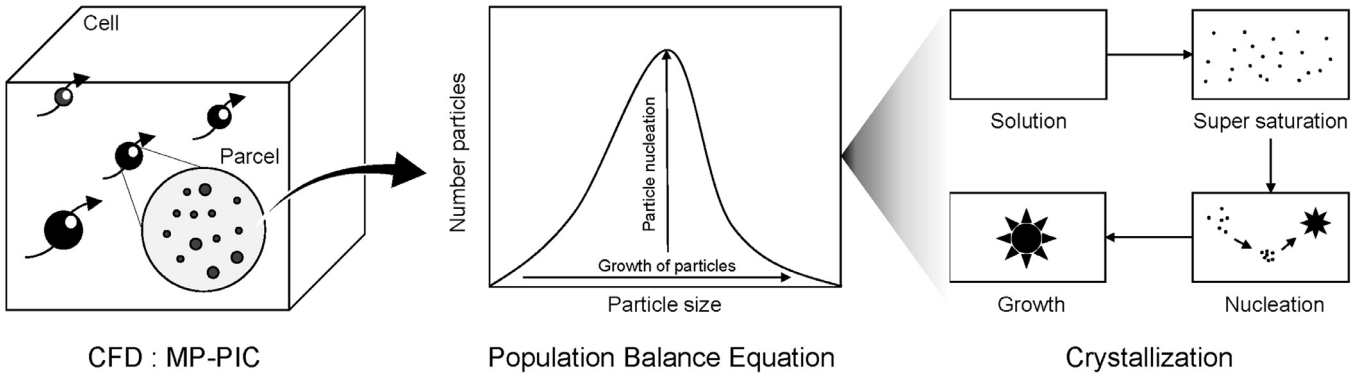


**Fig. 1.** Schematic diagram of the MP-PIC-PBE for a supersaturated crystallization.

This study proposes the multiphase particle-in-cell coupled with population balance equation (MP-PIC-PBE) method. This numerical simulation method can efficiently simulate the micro-scale particle distribution changes sensitive to fluid phase dynamics. The PBE is considered within a Lagrangian frame, to efficiently combine with the particle distribution function used in MP-PIC. This approach preserves mass and energy conservation between the phases in the Eulerian and Lagrangian frames. The PBE in this procedure is directly linked to the discrete parcels and retains all the original information while maintaining homogeneity. This characteristic makes the simulation of the particle distribution more efficient than for the PBE in an Euler-Eulerian approach.

For the antisolvent crystallization of Lovastatin in a biradial mixer, the proposed method is compared to the coupled CFD-PDF-PBE method, which predicts the particles' behavior and particle size distribution by combining a multi-environment probability density function (PDF) with the PBE in an Eulerian frame (da Rosa and Braatz, 2018; Pirkle et al., 2015; Woo et al., 2009, 2006). The MP-PIC-PBE method is consistent with the CFD-PDF-PBE method within the maximum difference of about 3.2%, while providing more information such as particle size, velocity, and location.

## 2. Model description

The proposed method is an extension of the MP-PIC method (Andrews and O'Rourke, 1996). The mass, momentum, energy, and species equations are solved for the continuous phase, and the Liouville equation (Williams, 1985) is solved for the particulate phase. The continuous phase is expressed as compressible flow since the model involves the density changes according to the components' mixing, mass transfer, and chemical reactions. The compressibility with the changing density is numerically computed based on the Reynolds time-averaging procedure (Holzmann, 2018).

The particulate phase is injected and tracked in a Lagrangian reference frame. The collisional force between particles are included using the continuum particle stress model (Harris and Crighton, 1994), and the interphase effect between the particulate phase and the continuous phase is represented by the drag force (Gidaspow, 1994). The particle normal stress can be changed according to the particles concentration of the system to be analyzed, and the drag force can be varied depending on the state of the continuous phase (gas, liquid, or solid) or by rearranging various parameters (Liu, 2018).

To simulate the particles' behavior in a reactor, the particles' size and mass changes including micro-scale phenomena should be predicted comprehensively. In this study, a computational fluid dynamics (CFD) approach is proposed for predicting the correlation between fluid dynamics on the mesoscale and particle distribution changes on the microscale, as shown in Fig. 1. This method solves the independent PBE for each parcel to reflect the physicochemical changes caused by the interaction with the continuous phase. A parcel is assumed to be a perfectly mixed reactor, and the homogeneous PBE predicts the particle distribution within a parcel. The PBE of a parcel includes the time and particle dimensions and can ignore the spatial dimension, which removes the convective and diffusive terms in the PBE, which are related to the Liouville equation in the MP-PIC method. In other words, in population dynamics, MP-PIC predicts the changes by the particle flow, and the independent homogeneous PBE reflects the changes by chemical sources. The calculation of the PBE on a parcel by parcel basis in the cell increases the numerical stability and reduces computational cost without eliminating relevant mathematical details.

### 2.1. Model equations of motion

#### 2.1.1. Continuous fluid phase

General equations of the continuous fluid phase reflecting momentum and energy balance due to mass change, considering compressible liquid density, can be described by

Mass equation

$$\frac{\partial\left(\theta_f\rho_f\right)}{\partial t}+\nabla\cdot\left(\theta_f\rho_f u_f\right)=-\mathrm{S}_m\,, \tag{1}$$

Momentum equation

$$\frac{\partial\left(\theta_f\rho_f u_f\right)}{\partial t}+\nabla\cdot\left(\theta_f\rho_f u_f u_f\right)+\nabla\cdot\tau = -\nabla\mathrm{P}+\theta_f\rho_f g-\mathrm{F}-u_f\mathrm{S}_m\,, \tag{2}$$

Energy equation

$$\frac{\partial\left(\theta_f\rho_f h_f\right)}{\partial t}+\nabla\left(\theta_f\rho_f u_f h_f\right)+\frac{\partial\left(\theta_f\rho_f K_f\right)}{\partial t} +\nabla\left(\theta_f\rho_f u_f K_f\right)-\theta_f\frac{\partial\mathrm{P}}{\partial t} = \nabla\cdot\theta_f\left[k_{eff}\nabla\mathrm{T}+\left(\overline{\overline{\tau}}_{eff}\cdot u_f\right)\right]+\theta_f\rho_f g\cdot u_f+\mathrm{S}_e\,, \tag{3}$$

Species equation

$$\frac{\partial\left(\theta_f\rho_f x_i\right)}{\partial t}+\nabla\cdot\left(\theta_f\rho_f u_f x_i\right)=\nabla\cdot\theta_f\rho_f\mathrm{D}\nabla x_i-\mathrm{S}_{m,i}\,, \tag{4}$$

where $\theta_f$ is the fluid volume fraction, $\rho_f$ is the fluid density, $u_f$ is the fluid velocity, $\mathrm{S}_m$ is the mass source, $\tau$ is the shear stress by viscous and turbulent flow, P is the system pressure, F is the interphase momentum transfer that includes viscous drag between particles and drag force between the particulate phase and the fluid phase, $u_f\mathrm{S}_m$ is the momentum source by mass transfer, $g$ is the gravitational acceleration, $h_f$ is the fluid enthalpy, $K_f=|u_f|^2/2$ is the kinetic energy, $k_{eff}$ is the fluid thermal conductivity, $\overline{\overline{\tau}}_{eff}\cdot u_f$ is

the mechanical source, $S_e$ is the energy source by mass transfer, $x_i$ is the mass fraction of component $i$, and D is the molecular diffusivity.

*2.1.2. Particulate phase*

The particulate phase equations based on MP-PIC are expressed by (Andrews and O'Rourke, 1996)

Particle distribution function

$$\frac{\partial f}{\partial t} + \nabla \cdot (f v_p) + \nabla_{v_p} \cdot (fA) = 0 \ , \tag{5}$$

Particle acceleration

$$\frac{\partial v_p}{\partial t} = \mathrm{A} = D_p\left(u_f - v_p\right) - \frac{1}{\rho_p}\nabla \mathrm{P} + g - \frac{1}{\theta_p \rho_p}\nabla \tau_p \ , \tag{6}$$

Particle drag function

$$D_p = \mathrm{C}_d \frac{3}{8}\frac{\rho_f}{\rho_p}\frac{\left|u_f - v_p\right|}{r} \ ,$$

where

$$\mathrm{C}_d = \frac{24}{\mathrm{Re}}{\theta_f}^{-2.65}\left(1 + 0.5\mathrm{Re}^{0.687}\right);\ \textit{if}\ \mathrm{Re} < 1000 \ ,$$

$$\mathrm{C}_d = 0.44\,{\theta_f}^{-2.65};\ \textit{if}\ \mathrm{Re} \geq 1000 \ ,$$

$$\mathrm{Re} = \frac{2\rho_f |u_f - v_p| r}{\mu_f} \ . \tag{7}$$

Isotropic interparticle stress

$$\tau = \frac{P_s {\theta_p}^{\beta}}{\max\left\{\theta_{cp} - \theta_p,\ \varepsilon(1-\theta_p)\right\}} \ , \tag{8}$$

Particle volume fraction

$$\theta_p = \int\int^{f} \frac{m}{\rho_p} dm dv \ , \tag{9}$$

Liquid volume fraction

$$\theta_f + \theta_p = 1 \ , \tag{10}$$

Interphase momentum transfer function

$$\mathrm{F} = \int\int^{f} m\left[D_p\left(u_f - v_p\right) - \frac{1}{\rho_p}\nabla \mathrm{P}\right] dm\, dv \ , \tag{11}$$

where $f$ is the particle distribution function in the Euler grid, $v_p$ is the discrete particle velocity, A is the discrete particle acceleration, $D_p$ is the particle drag function, $C_d$ is the drag coefficient, $r$ is the particle mean radius, $\tau_p$ is the interparticle stress, $P_s$ is a constant in units of pressure, $\theta_p$ and $\theta_{cp}$ are the particle volume fraction and its maximum, $m$ is the total mass of the particles in a parcel, $\beta$ is a constant whose value is recommended between 2 and 5, and $\varepsilon$ is a small number on the order of $10^{-7}$ (Snider, 2001). The particle mean radius and the total mass of the particles are solved by the PBE in each parcel.

*2.2. Population balance equation in a parcel*

The general form of PBE reflecting the interaction between particles and external influences is represented by (Woo et al., 2006)

$$\frac{\partial N_j}{\partial t} + \nabla \cdot \left(N_j v_p\right) - \nabla \cdot D_t \nabla N_j \cdot = -\sum_j \frac{\partial\left[G_j\left(r_j, c, T\right)\right]}{\partial r_j} + B\left(N_j, c, T\right)\prod_j \delta\left(r_j - r_{j0}\right) + h\left(N_j, c, T\right) \ , \tag{12}$$

where $N_j$ is the particle number density within a parcel, $D_t$ is the local turbulent diffusivity, $G_j(r_j, c, T)$ is the growth rate, $r_j$ is the particle internal coordinate, $r_{j0}$ is the particle internal coordinate for a crystal nucleus, $\delta$ is the Dirac delta function, $B(N_j, c, T)$ is the nucleation rate, and $h(N_j, c, T)$ is the creation or destruction of particles due to aggregation, agglomeration, and breakage.

Since the case study used for demonstration later involves crystallization, in this work, the PBE needs to express only the nucleation and growth of particles. Also, since each parcel is assumed to be well mixed and tracked independently in the Lagrangian frame, the convective and diffusive terms for the particles over the spatial domains in Eq. (12) disappear, and the PBE reduces to

$$\frac{\partial N_j}{\partial t} = -\sum_j \frac{\partial\left[G_j\left(r_j, c, T\right)\right]}{\partial r_j} + B\left(N_j, c, T\right)\prod_j \delta\left(r_j - r_{j0}\right) \ . \tag{13}$$

If the various source terms $h(N_j, \rho_i, T)$ is added in Eq. (13) as in Eq. (12), the model can be used for various applications such as polymerization, milling, and fluidized bed (Ramkrishna, 2000; Ramkrishna and Singh, 2014; Rigopoulos, 2010).

The $N_j$ of a parcel expressed in Eq. (13) represents the particle distribution of the parcel in the cell where the parcel is located. With $N_j$, the total mass of a parcel and the average particle size can be calculated by

$$N_{w,j} = \rho_p k_v \int^{r^3} N_j dr \ , \tag{14}$$

$$m = V_{cell}\sum_j N_{w,j} \ , \tag{15}$$

$$r = \frac{D_{43}}{2} \ ,$$

where

$$D_{43} = \frac{\sum_j N_{w,j} r_j^4}{\sum_j N_{w,j} r_j^3} \ , \tag{16}$$

$N_{w,j}$ is the average particle mass per cell volume, $k_v = 6.25 \times 10^{-4}$ is the volume shape factor (Pirkle et al., 2015), $V_{cell}$ is the volume of the cell where the particle is positioned, and $D_{43}$ is the volume mean diameter of particles in a parcel.

The cell volume $V_{cell}$ used in Eq. (15) has a special mathematical and numerical meaning. The nucleation rate and growth rate of the PBE in the parcel, expressed mathematically in Eq. (13), are functions of the concentration and temperature of the fluid phase. Eq. (15) exchanges mass and energy according to the information about the fluid phase in the cell where the parcel is located. The generated particles are expressed as the total particles mass in a parcel per located cell volume $\sum_j N_{w,j}$. Therefore, Eq. (15) is a step of converting an intensive variable $\sum_j N_{w,j}$ to an extensive variable $m$. When the transformed $m$ is applied to Eqs. (9) and (11), the particle mass change of a parcel by the PBE can be reflected in the particle distribution calculation. Based on this approach, governing variables such as mass, momentum, and energy can be made consistent with particle changes. The particle distributions in the Lagrangian frame are computed simultaneously in the Eulerian mesh domain tracked in the continuous fluid phase based on PIC (Harlow and Amsden, 1971). This approach allows the minimization of the numerical inconsistency between the Lagrangian phase and the continuous phase by the PBE.

*2.3. Numerical solution*

*2.3.1. Particulate phase*

In computation, a parcel contains a number of particles with identical mass, velocity, and position. The conservation of particles by dynamic motion in the particulate phase is represented by the

Liouville Eq. (5). Parcel position and velocity are updated implicitly by

$$x_p^{n+1} = x_p^n + \Delta t\, v_p^{n+1} \ , \tag{17}$$

$$v_p^{n+1} = \frac{v_p^n + \Delta t\left(D_p\, u_{f,p}^{n+1} - \frac{1}{\rho_p}\nabla \mathrm{P}_p^{n+1} - \frac{1}{\rho_p \theta_p}\nabla \tau_p^{n+1} + g\right)}{1 + \Delta t\, D_p} \ , \tag{18}$$

where $x_p$ is the parcel (particles) position, and $u_{f,p}^{n+1}$, $\nabla \mathrm{P}_p^{n+1}$, and $\nabla \tau_p^{n+1}$ are the fluid velocity, the pressure gradient, and the inter-particle stress gradient interpolated implicitly at the particle location (Snider, 2001).

The PBE calculates particle size and mass changes within a parcel. The particle information updated by the PBE is reflected in the particulate phase, and multiphase fluid dynamics calculation ensues. Although the homogeneous PBE independent of the spatial domain is used, using too many parcels may incur significant cost for the PBE calculations, because the number of ordinary differential equations to be solved increases with the particle dimension $j$ and the number of parcels. The high-resolution central scheme provides an environment where a sufficiently large $\Delta r$ could be used LeVeque, 2002). The PBE is rewritten by combining Eqs. (13) and ((14) on a mass basis to give

$$\frac{dN_{w,j}}{dt} = S_{m,j} = \begin{cases} \dfrac{\rho_p k_v}{4\Delta r}\left[\left(r_{j+1/2}\right)^4 - \left(r_{j-1/2}\right)^4\right]\left\{\begin{array}{l} -G_{j+1/2}\left[N_j + \dfrac{\Delta r}{2}(N_r)_j\right] \\ \quad +G_{j-1/2}\left[N_{j-1} + \dfrac{\Delta r}{2}(N_r)_{j-1}\right] + \underbrace{B}_{j=0} \end{array}\right\}; & \text{if } G < 0 \\ \dfrac{\rho_p k_v}{4\Delta r}\left[\left(r_{j+1/2}\right)^4 - \left(r_{j-1/2}\right)^4\right]\left\{\begin{array}{l} -G_{j+1/2}\left[N_{j+1} - \dfrac{\Delta r}{2}(N_r)_{j+1}\right] \\ \quad +G_{j-1/2}\left[N_j - \dfrac{\Delta r}{2}(N_r)_j\right] \end{array}\right\}; & \text{if } G > 0 \end{cases} \tag{19}$$

and is evaluated in the finite particle domain between size $r_{j+1/2}$ and $r_{j-1/2}$, where $(N_r)_j$ is the particle number density which is approximated by the minmod limiter, the nucleation rate $B$ is the involved in the generation of the smallest particles, $G > 0$ means particle growth, and $G < 0$ means particle dissolution. The reader is referred to the reference for details on the high-resolution discrete central schemes for the solution method of population balance (Woo et al., 2006).

In crystallization, the molecular components exchange only the solute between the Eulerian and Lagrangian frames. Therefore, the mass source is expressed by $S_m = \sum_j \sum_k S_{m,j,k}$, where $k$ represents the number of parcels that can be tracked within a Euler grid.

### 2.3.2. Continuous fluid phase

Volume fractions of the phases are calculated explicitly by particulate phase Eqs. (9) and (10). Then, the continuous fluid phase equations of (1)–(4) are solved implicitly by coupling particles with fluid, and the calculated continuous fluid properties are interpolated back to the particle positions. At this time, the continuous fluid phase is approximated using the finite volume method in the Eulerian frame, developed in Cartesian coordinates. To solve the Eulerian frame equations, the PIMPLE (Merged PISO-SIMPLE) algorithm is applied which is a combination of PISO (Pressure Implicit with Splitting of Operator) and SIMPLE (Semi-Implicit Method for Pressure-Linked Equations) (Issa, 1986; Patankar, 1980). The numerical approximation equations according to the PIMPLE algorithm procedure are:

Step 1. Define and solve the discretized momentum equation by Eq. (2),

$$u_{f,c} = \frac{H\left(u_f\right)}{a_c} - \frac{\nabla \mathrm{P}_c}{a_c} \ , \tag{20}$$

where

$$H\left(u_f\right) = -\sum_{+\theta_{f,c}\rho_{f,c}g_c}^{a_{nb}} u_{f,nb} + \sum^{(\mu_{eff})_s} \left|\vec{s}_s\right| \cdot \vec{k}\,\left(\nabla u_{f,c}\right)_s - F_c + u_{f,c} S_{m,c} \ .$$

Step 2. Define and solve the pressure correction equation by Eq. (1),

$$\nabla \frac{\theta_{f,c}}{a_c}\nabla P_c - \theta_{f,c}\psi\left(\frac{dP_c}{dt} - \frac{dP_c^o}{dt}\right) = \frac{d\theta_{f,c}\rho_{f,c}}{dt} + \nabla \cdot \theta_{f,c}\rho_{f,s}\vec{s}_s\left(\frac{H\left(u_f\right)}{a_c}\right)_s + S_{m,c} \ . \tag{21}$$

Step 3. Correct the flux

$$\hat{\phi}_s = \vec{s}_s\left(\frac{H\left(u_f\right)}{a_c}\right)_s + \frac{P_s \vec{s}_s}{\rho_{f,s}} \ . \tag{22}$$

Step 4. Perform the momentum corrector step using Eq. (20).

Step 5. Update density-reflected compressibility,

$$\rho_f = \rho_f' + \left(\psi P - \psi' P'\right),$$

where

$$\psi = \frac{\rho_f}{P}, \ \frac{1}{\rho_f} = \sum_i x_i \frac{1}{\rho_{f,i}} \ . \tag{23}$$

Repeat Steps 2 to 5 for the corrector steps.

In the above equations, the subscript c expresses the center variables of the cell volume, the subscript s expresses interpolated surface variables, the subscript nb expresses neighbor variables of the cell volume, the superscript o expresses previous time step variables, the superscript $'$ expresses previous iteration step variables, $a_c$ and $a_{nb}$ are diagonal coefficients of the velocity matrix, $\mu_{eff}$ is the effective viscosity and is implemented in turbulent models, $\vec{s}_s$ is the surface area operator, $\vec{k}$ is the bulk viscosity, $\psi$ is the liquid compressibility, and $\hat{\phi}_s$ is the face flux. The term $H(u_f)$ consists of matrix coefficients of the neighboring cells multiplied by their velocity, and source terms except for the pressure gradient such as diffusion, gravity, interphase momentum transfer, and molecular mass transfer terms. The corrector steps are user-specified parameters that can be specified in order for the system to obtain an efficient calculation time.

The proposed numerical simulation method was implemented on OpenFOAM 5.0 and was developed based on DPMFoam

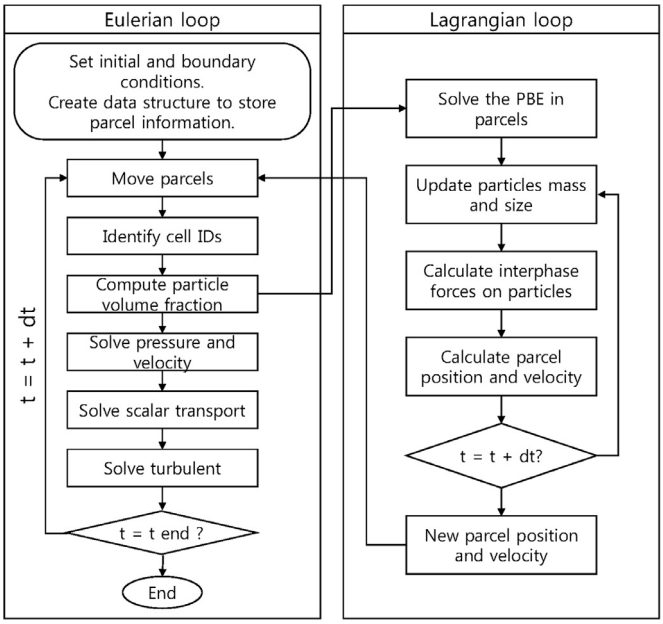


**Fig. 2.** Schematic diagram of the numerical solution procedure.

(Fernandes et al., 2018). The reader is referred to the references for details on the Eulerian frame solution method using the PIMPLE algorithm on OpenFOAM (Holzmann, 2018; Moukalled et al., 2015). Fig. 2 shows the schematic diagram of the numerical solution procedure of the developed method.

## 3. Description of the Simulation Case Study

### 3.1. CFD-PDF-PBE method

In the CFD field, the probability density function (PDF) method is used to predict the micromixing of fluids by approximating distributions measured through experiments. This method is mainly used in turbulent combustion modeling, and the beta probability function model is the most popular choice (Pope, 1985). The CFD-PDF-PBE is a multi-scale CFD modeling method (2006) that analyzes the turbulent flow pattern using CFD, solves the micromixing in the sub-grid scale using the multi-environment probability density function, and evaluates the particle size distribution using the population balance equation.

The MP-PIC-PBE method has mainly four advantages over the CFD-PDF-PBE method: (1) enhanced generality, (2) lower computational cost, (3) improved accuracy due to the accounting of collisions and drag forces, and (4) more tracked information on the particles. First, the MP-PIC-PBE method has a first-principles model of micromixing. As such, the method can be used in a variety of systems without resorting to a statistical model, which must be developed for each specific case. Secondly, the use of the homogeneous PBE enables a more computationally efficient prediction of PSD compared to the 4-dimensional (3D Cartesian domain + 1D particle domain) PBE, because the homogeneous PBE does not contain derivatives with respect to the 3D Cartesian domain. Although the computational cost of the Lagrangian frame is more expensive than the Eulerian frame in general, the MP-PIC using parcels can be cheap because it requires less memory for tracking than the discrete element method. Also, the Euler-Lagrangian method can be made numerically more stable than the Euler-Euler method because the two phases are segregated and solved numerically (Andrews and O'Rourke, 1996). Thirdly, the collision between particles and the drag force between particles and fluid are taken into account to predict the flow of particles more accurately. Lastly, the Lagrangian frame predicts more unmeasurable variables of particles such as particle age, particle streamline, and particle position. If the prediction of the behavior of free-flowing particles is desired, the choice of the Lagrangian frame is a good approach.

In this work, simulation results are compared for the MP-PIC-PBE and CFD-PDF-PBE methods for a highly nonlinear crystallization process. In this comparison, the underlying models are matched to the best possible extent within the available information. For example, the standard k-epsilon model of the Reynolds-averaged Navier-Stokes model is used for turbulent energy. However, thermophysical models have some differences as CFD-PDF-PBE uses the ideal mixture model whereas MP-PIC-PBE uses the multi-component mixture model. In MP-PIC-PBE, various thermophysical properties due to molecular composition changes are predicted by a mixing rule. Additionally, the MP-PIC-PBE includes compressible liquid density and reflects the various scalar transport models in the species transport. Table 1 compares the models used in MPPIC-PBE and CFD-PDF-PBE.

### 3.2. Process description

The two methods are used to simulate a solution crystallizer producing Lovastatin crystals studied using CFD-PDF-PBE by da Rosa & Braatz (2018). The crystallizer is a biradial tubular mixer in which two antisolvent inlets are vertically inserted, and a solution (Lovastatin solvent + methanol) is injected into the main inlet. The computational domain used for the simulation is shown in Fig. 3. MP-PIC-PBE based on the Lagrangian frame cannot take advantage of symmetry in the domain, because the particulate phase needs to know all the coordinates of the system domain to be tracked. The computational domain is drawn in full 3D, and the mesh comprises 153,629 cells in total. For the particulate phase, 100,000 massless parcels per second are injected into the main inlet. Since the average residence time of the particles is about 1.5 s, about 150,000 parcels remain in the system during the calculation. The number of parcels is similar to the number of cells in the computation domain used. There is a trade-off in simulation accuracy between the number of parcels and the number of particles. Lowering the particle number within a parcel may improve the simulation accuracy of the fluid dynamics, but could require a higher parcel number. On the other hand, the MP-PIC-PBE method imple-

**Table 1**
Comparison of the general models used in the two solvers compared.

| | MP-PIC-PBE | CFD-PDF-PBE |
|---|---|---|
| Particle motion | Lagrangian frame | Euler frame |
| Compressibility | Applied | Ignored |
| Heat of mixing | Realistic enthalpy | Rate based (by PDF) |
| Species transport | First-principles-based scalar transport model | PDF |
| Particulate momentum transfer | Particles collision and drag force | Ignored (but included in the PDF) |
| Turbulent | RANS k-epsilon | RANS k-epsilon |
| Thermophysical properties + Antisolvent | Multi-component mixture | Ideal mixture (solution) |

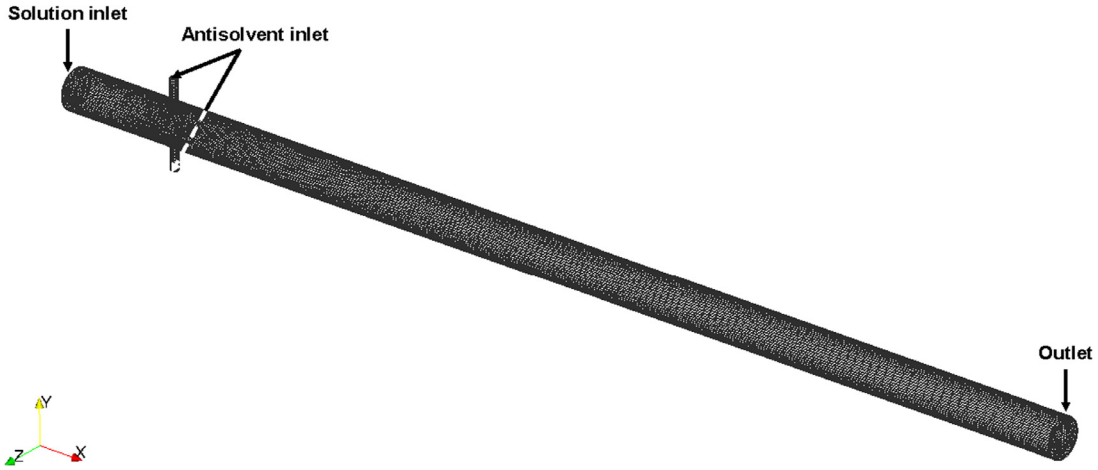


**Fig. 3.** Illustration of the computational domain for a radial crystallizer.

**Table 2**
Design parameters and operating conditions used in the simulations.

| | Variable | | | Value | Unit |
|---|---|---|---|---|---|
| Design parameters | Number of antisolvent inlets | | | 2 | # |
| | Diameter of antisolvent inlet | | | 0.007147 | m |
| | Diameter | | | 0.0363 | m |
| | Length | | | 1 | m |
| Operating conditions | Antisolvent (water) inlet | Flow rate | 0.48 | kg/s | |
| | | Temperature | 293.15 | K | |
| | Solution inlet | Flow rate | Solvent | 0.028 | kg/s |
| | | | Methanol | 0.528 | kg/s |
| | | Temperature | 305.00 | K | |
| | Pressure | | | 1 | bar |

ments a micro-scale particle distribution in parcels as the PBE to achieve the simulation accuracy needed, we recommend maintaining the particle number as closely as possible to the experimental particle sample. The detailed design parameters and operating conditions of the process are listed in Table 2.

### 3.3. Kinetics of crystallization

The crystallization kinetics of Lovastatin are taken from Pirkle et al. (2015). The solubility was fitted as a function of temperature and antisolvent weight percent, and nucleation and growth rates are calculated as functions of the solubility:

$$B = B_{homogeneous} + B_{heterogeneous} \ ,$$

where

$$B_{homogeneous} \text{ at } 296.15 \text{ K } \left(\#/\text{m}^3\text{s}\right) = 6.97 \ \times 10^{14} \exp\left[\frac{-15.8}{(\ln S)^2}\right] ,$$

$$B_{heterogeneous} \text{ at } 296.15 \text{ K } \left(\#/\text{m}^3\text{s}\right) = 2.18 \ \times 10^{8} \exp\left[\frac{-0.994}{(\ln S)^2}\right] \quad (24)$$

$$G \text{ at } 296.15 \text{ K } (\text{m/s}) = 8.33 \ \times 10^{-30} \left(2.46 \ \times 10^{3} \ln S\right)^{6.7} , \quad (25)$$

where

$$S = \frac{c}{c^*} \ .$$

where

$$\eta = \frac{T}{T_{ref}}, \ T_{ref} = 296.15 \text{ K} \ ,$$

$B$ is the nucleation rate, $S$ is the relative supersaturation, $c$ and $c^*$ are the solute concentration and the solubility, $\eta$ is the dimensionless temperature, and $T_{ref}$ is the reference temperature.

This crystallization of Lovastatin induces supersaturation using an antisolvent, which involves two exotherms. One exotherm is the heat of mixing which is caused by the mixing of methanol and water, which is the enthalpy change caused by the thermodynamic change due to the ionization of organic acids and linear free energy relations of the solution, and can be fitted as a function of the water ratio in the solution which was taken from Bertrand et al. (1966). Realistic enthalpy can be calculated as the sum of the ideal enthalpy and the enthalpy change by mixing:

$$h_f = h_{f,ideal} + h_{f,mix} \ . \quad (27)$$

Another exotherm is the heat of crystallization $h_{f,crys} =$ 38042.5 kJ/kmol (Pirkle et al., 2015). This enthalpy change caused by crystallization can be expressed in terms of the rate-based heat source:

$$S_e = h_{f,crys} S_m \ . \quad (28)$$

$$c^*\left(\frac{\text{kg}}{\text{kg of solvents}}\right) = 0.001 \exp\left(15.45763\left(1 - \frac{1}{\eta}\right)\right) + \begin{cases} -2.7455 \ \times 10^{-4} W_{as}^3 + 3.3716 \ \times 10^{-2} W_{as}^2 - 1.6704 W_{as} \\ \quad +33.089 \ ; \ if \ W_{as} \le 45.67\% \\ -1.7884 \ \times 10^{-2} W_{as} + 1.7888 \ ; \ if \ W_{as} > 45.67\% \end{cases} \quad (26)$$

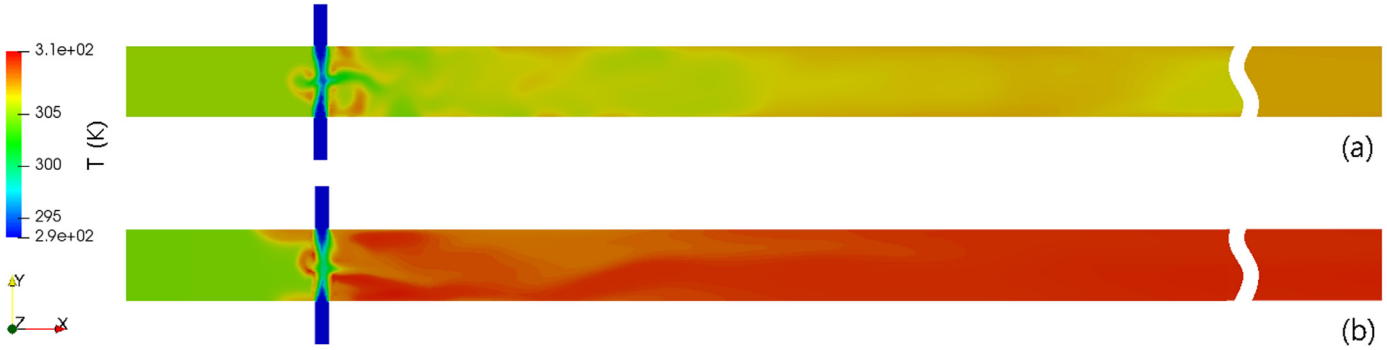


**Fig. 4.** Temperature field: (a) CFD-PDF-PBE; (b) MP-PIC-PBE.


**Fig. 5.** Solute (Lovastatin) mass fraction field: (a) CFD-PDF-PBE; (b) MP-PIC-PBE.


**Fig. 6.** Growth rate field: (a) CFD-PDF-PBE; (b) MP-PIC-PBE.

## 4. Results and Discussion

### *4.1. Validation*

MP-PIC-type methods have been used and verified in a variety of fluid dynamical systems. This article evaluates the MP-PIC-PBE for particle nucleation and growth. The quasi-steady results are compared quantitatively and qualitatively. Since the residence time of the system is about 1 s (da Rosa and Braatz, 2018), the results at 7 s after the start of the simulation was treated as being quasi-steady.

To evaluate the effect of the heat of mixing and the heat of crystallization, the temperature field within the system is shown in Fig. 4. The 305 K solution and the 298.15 K antisolvent are injected at the main inlet and at the radial inlets respectively. Near the radial inlets, the first contact between the solution and the antisolvent causes a fast rise in temperature due to the heat of mixing. The change in solvent compositions results in crystal nucleation and growth, which releases heat of crystallization. At this location, the maximum temperatures for the two methods are observed at (a) 309.21 K and (b) 310.34 K respectively. Mixing occurs continuously through to the crystallizer outlet, inducing further energy change. The average temperature at the crystallizer outlet is calculated as (a) 307.41 K and (b) 310.10 K, respectively. The MP-PIC-PBE temperature is about 2 to 3 K higher at all locations downstream of the radial inlets. The basic thermodynamic calculation of the temperature change caused by the heat of mixing showed 309.47 K under the perfect mixing assumption. Considering that the temperature rose by 0.5 K due to the heat of crystallization in da Roas & Braatz (2018), the MP-PIC-PBE outlet temperature is closer to the thermodynamic calculation than for CFD-PDF-PBE. The underestimation of the heat of mixing in the CFD-PDF-PBE is associated with the two methods using fundamentally different models to express the heat of mixing. CFD-PDF-PBE assumes that the solution (solvent + antisolvent) is an ideal mixture. Instead of using a realistic enthalpy expression, the rate-based heat of mixing is represented in the PDF.

The temperature fields of the two methods have qualitative similarities. A dramatic turbulence flow due to the convective force and intense mixing of the components are observed near the radial inlets. After the intense mixing, the heat was dissipated in the direction of the outlet by convection and diffusion.


**Fig. 7.** Nucleation rate field: (a) CFD-PDF-PBE; (b) MP-PIC-PBE.

**Table 3**
Area-average crystal size, and solute conversion at the outlet.

| | Average crystal size ($\mu$m) | Solute conversion (%) |
|---|---|---|
| MP-PIC-PBE | 132.51 | 73.30 |
| CFD-PDF-PBE | 136.78 | 71.56 |

The solute mass fraction field in the liquid is similar for the two methods (Fig. 5). The liquid solute is a sensitive variable in the scalar transport phenomena due to various physicochemical changes, such as mixing by injection, precipitation by supersaturation, and molecular diffusion. MP-PIC-PBE whose scalar transport is based on first principles predicts similar results CFD-PDF-PBE whose scalar transport is based on the presumed PDF model. The average mass fraction at the outlets are (a) 0.00768, and (b) 0.00721. More solute molecules have been converted to solid in MP-PIC-PBE. MP-PIC-PBE has higher asymmetry upstream of the radial inlets, and better mixing of the solvent immediately downstream of the radial inlets.

The crystallization rates show the same qualitative trend of being high near the antisolvent injection, and low at about halfway down the tube (see Figs. 6 and 7). The maximum growth rates are (a) $1.778 \times 10^{-3}$, and (b) $1.737 \times 10^{-3}$ m/s, and the maximum nucleation rates are (a) $1.85 \times 10^{14}$, and (b) $1.84 \times 10^{14}$ #/m$^3$s. The crystallization rates near the injection antisolvent are quantitatively different. The crystallization rates are higher in the center between the radial inlets for CFD-PDF-PBE than for MP-PIC-PBE because the underestimated heat of mixing of the former predicted lower temperatures leading to lower solubilities. Despite the lower solubilities in CFD-PDF-PBE, more solute molecules were converted to the solid phase in MP-PIC-PBE in the crystallizer due to differing hydrodynamic predictions by the two methods.

The crystal size distribution (CSD) was analyzed in terms of the mass-weighted average and the number-weighted average at the outlet of the crystallizer. MP-PIC-PBE produced a narrower CSD (Fig. 8a). More crystals at about 160 microns and about 25 microns indicate that CFD-PDF-PBE had higher early and late nucleation (Fig. 8a,b), which was due to the lower solubility. Table 3 summarizes the average size of the particles predicted by the two methods and the conversion of solute molecules to particles, which was smaller and higher respectively for MP-PIC-PBE. The two methods use different multi-phase mixing models, which would be expected to contribute to the different particle distribution and solute conversion.

Table 4 shows relative differences in the quantitative comparison of the two methods. MP-PIC-PBE gives results that match those of CFD-PDF-PBE within the maximum difference range of 3.2%.

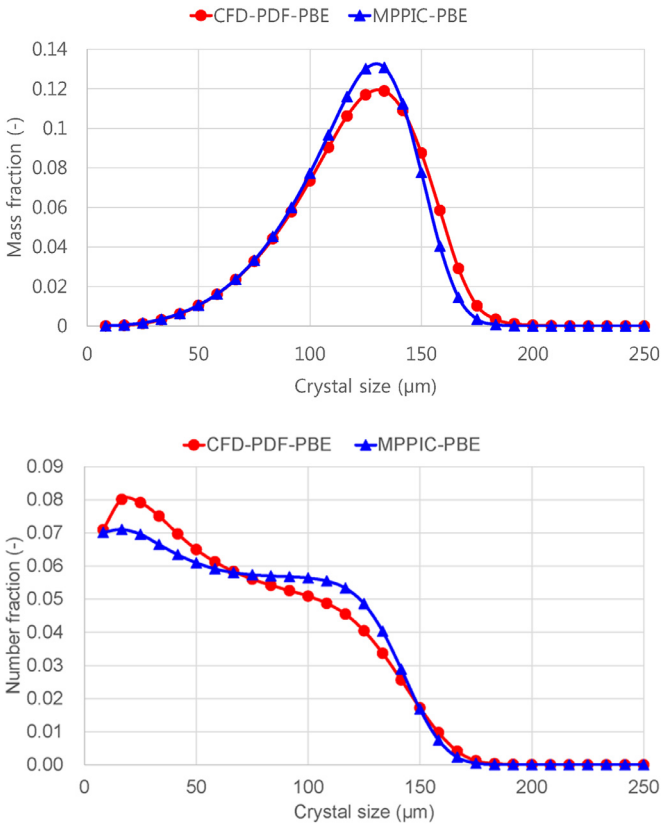


**Fig. 8.** Crystal size distribution at the outlet: (a) mass-weighted average; (b) number-weighted average.

### 4.2. Evaluation of MP-PIC-PBE

As mentioned in Section 3.1, the proposed CFD method has some advantages arising from the use of the Lagrangian frame and the homogeneous PBE. Fig. 9 shows the variables that are outputs of MP-PIC-PBE but not CFD-PDF-PBE. First, the age of the particles can be outputted. From a particle's age, its residence time, i.e. time duration from when a particle is injected into the system to when it escapes, can be obtained. The residence time for the radial crystallizer was estimated by this approach to be about 1.5 s. The age of parcels is powerful when the system has a complex flow pattern, and the particles behave discontinuously. The number of particles and the size of the particles, in a parcel, can also be simulated as shown in Fig. 9b,c. These variables show significant radial spatial heterogeneity in the crystallizer. At the crystallizer outlet, the large particles are preferentially located near one wall whereas

**Table 4**
Relative differences in the evaluated variables.

| | Temperature | Solute conversion | Mean crystal size | Maximum growth rate | Maximum nucleation rate |
|---|---|---|---|---|---|
| Relative difference | 0.9% | 2.4% | 3.2% | 2.4% | 0.5% |

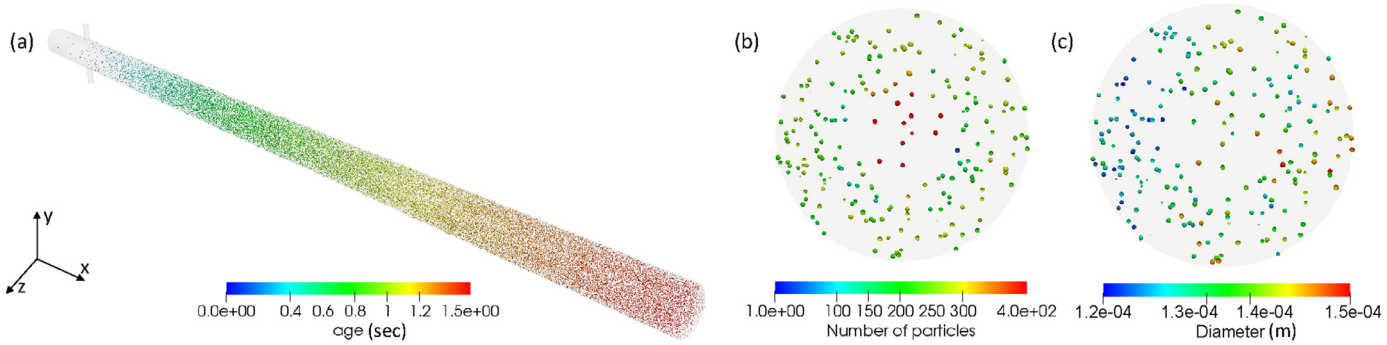


**Fig. 9.** Additional particle information predicted by MP-PIC-PBE: (a) particle age; (b) number of particles in parcels; (c) mean diameter of parcels.

the small particles preferentially near the opposite wall. The trend is due to a screw flow pattern formed in the cylindrical crystallizer (see Figs. 4, 6, 7) leading to active mixing of the liquid solute and antisolvent in the reactor center that is not captured by CFD-PDF-PBE. The screw flow distributes relatively small particles toward a crystallizer wall.

The main disadvantage of MP-PIC-PBE is that using parcels can degrade the accuracy of the particulate flow at high particle densities. In particular, the parcel size cannot be larger than the Euler grid. Although the accuracy can be improved by adjusting the simulation parameters according to the number of particles in a parcel (Benyahia and Galvin, 2010), this adjustment represents a slight inconvenience in using MP-PIC-PBE. If the user can overcome this basic limitation of MP-PIC, MP-PIC-PBE is a beneficial solution for predicting multi-scale particulate flows with particle size variation.

As mentioned before, the combination of the Lagrangian frame and PBE is expected to improve the numerical solubility and reduce the computational cost. Technically the computational efficiency of the two methods cannot be directly compared due to their difference in the mathematical form and the numerical solution method. However regarding the simulation time using one Core of Intel (R) CPU of I7-6700 3.40 GHz, MP-PIC-PBE required about 9 h while CFD-PDF-PBE requires about 30 h to obtain a real-time result of 1 s when optimized for numerical stability. If the volume of a cell is larger than the volume of a parcel, the cell size and the number of cells do not significantly affect the PBE calculation time.

## 5. Conclusion

MP-PIC-PBE is an extension of MP-PIC to predict multi-scale fluid phenomena, namely, combining micro-scale particle formation phenomena with meso-scale fluid mechanics. The method employs the PBE in homogeneous form, while maintaining equivalence with the full dimensional population balance equation. This proposed simulation method allows the particulate phase to express particulate stresses using spatial gradients, and adopts a Lagrangian description to predict particle properties such as mass, size, age, and velocity that are changed by the PBE. This approach is robust and relatively fast numerically in predicting particle size distributions with particulate fluid dynamics.

This article explains the fundamental equations and numerical solution methods of MP-PIC-PBE and compares the method to the existing solver called CFD-PDF-PBE. The test problem of crystallization demonstrates the advantages of MP-PIC-PBE in handling the particle size distribution. For variables that are computable by the two methods, the results are qualitatively similar but quantitatively different due to the various differences in the models employed. MP-PIC-PBE generates additional information not provided by CFD-PDF-PBE.

MP-PIC-PBE is a robust numerical framework for predicting and analyzing the various interactions between microscale physicochemical changes of particles and fluid dynamics variables that are expected to be useful in a variety of particulate systems. The technical details regarding the software can be found online (https://github.com/KAIST-LENSE/mppicPbeCryFoam)

## Declaration of Competing Interest

The authors declare that they have no known competing financial interests or personal relationships that could have appeared to influence the work reported in this paper.

## References

Andrews, M.J., O'Rourke, P.J., 1996. The multiphase particle-in-cell (MP-PIC) method for dense particulate flows. Int. J. Multiphase Flow 22, 379–402.
Benyahia, S., Galvin, J.E., 2010. Estimation of numerical errors related to some basic assumptions in discrete particle methods. Ind. Eng. Chem. Res. 49, 10588–10605.
Bertrand, G.L., Millero, fJ, Wu, C., Hepler, L.G., 1966. Thermochemical investigations of the water-ethanol and water-methanol solvent systems. I. heats of mixing, heats of solution, and heats of ionization of water. J. Phys. Chem. 70, 699–705.
Rosa, da, A., C., Braatz, R.D., 2018. Multiscale modeling and simulation of macromixing, micromixing, and crystal size distribution in radial mixers/crystallizers. Ind. Eng. Chem. Res. 57, 5433–5441.
Ding, J., Gidaspow, D., 1990. A bubbling fluidization model using kinetic-theory of granular flow. AIChE J. 36, 523–538.
Fernandes, C., Semyonov, D., Ferras, L.L., Nbrega, J.M., 2018. Validation of the CFD-DPM solver DPMFoam in OpenFOAM (R) through analytical, numerical and experimental comparisons. Granul. Matt. 20.
Gidaspow, D., 1994. Multiphase Flow and fluidization: Continuum and Kinetic Theory Descriptions. Academic Press, Boston.
Goldschmidt, M.J.V., Beetstra, R., Kuipers, J.A.M., 2004. Hydrodynamic modelling of dense gas-fluidised beds: comparison and validation of 3D discrete particle and continuum models. Powder Technol. 142, 23–47.
Harlow, F.H., & Amsden, A.A. (1971). Fluid dynamics: a LASL monograph. National Technical Information Service: U.S. Department of Commerce.
Harris, S.E., Crighton, D.G., 1994. Solutions, solitary waves and voidage disturbances in gas-fluidized beds. J. Fluid Mech. 266, 243–276.
Holzmann, T., 2018. Mathematics, numerics, derivations and OpenFOAM(r). Holzmann CFD.
Issa, R.I., 1986. Solution of the implicitly discretized fluid-flow equations by operator-splitting. J. Comput. Phys. 62, 40–65.

Khopkar, A.R., Kasat, G.R., Pandit, A.B., Ranade, V.V., 2006. Computational fluid dynamics simulation of the solid suspension in a stirred slurry reactor Ind. Eng. Chem. Res. 45, 4416–4428.
LeVeque, R.J., 2002. Finite Volume Methods for Hyperbolic Problems. Cambridge University Press.
Marchisio, D.L., Fox, R.O., 2005. Solution of population balance equations using the direct quadrature method of moments. J. Aerosol Sci. 36, 43–73.
Marchisio, D.L., Pikturna, J.T., Fox, R.O., Vigil, R.D., Barresi, A.A., 2003. Quadrature method of moments for population-balance equations. AIChE J. 49, 1266–1276.
Moukalled, F., Mangani, L., Darwish, M., 2015. The Finite Volume Method in Computational Fluid Dynamics, 113. Academic Press, Boston.
O'Rourke, P.J., 1981. Collective Drop Effects on Vaporizing Liquid Sparys. Princeton University.
O'Rourke, P.J., Brackbill, J.U., Larrouturou, B., 1993. On particle grid interpolation and calculating chemistry in particle-in-cell methods. J. Comput. Phys. 109, 37–52.
Patankar, S.V., 1980. Numerical Heat Transfer and Fluid Flow. McGraw-Hill.
Pirkle, C., Foguth, L.C., Brenek, S.J., Girard, K., Braatz, R.D., 2015. Computational fluid dynamics modeling of mixing effects for crystallization in coaxial nozzles. Chem. Eng. Process. 97, 213–232.
Pope, S.B., 1985. Pdf methods for turbulent reactive flows. Prog. Energy Combust. Sci. 11, 119–192.
Ramkrishna, D., 2000. Population balances: Theory and Applications to Particulate Systems in Engineering. Academic Press.
Ramkrishna, D., Singh, M.R., 2014. Population balance modeling: current status and future prospects. Annu. Rev. Chem. Biomol. Eng. 5 (5), 123–146.
Rigopoulos, S., 2010. Population balance modelling of polydispersed particles in reactive flows. Prog. Energy Combust. Sci. 36, 412–443.
Snider, D.M., 2001. An incompressible three-dimensional multiphase particle-in-cell model for dense particle flows. J. Comput. Phys. 170, 523–549.
Snider, D.M., O'Rourke, P.J., Andrews, M.J., 1998. Sediment flow in inclined vessels calculated using a multiphase particle-in-cell model for dense particle flows. Int. J. Multiphase Flow 24, 1359–1382.
Williams, F.A., 1985. Combustion Theory: the Fundamental Theory of Chemically Reacting Flow Systems, (2nd ed) Benjamin/Cummings Pub. Co.
Woo, X.Y., Tan, R.B.H., Braatz, R.D., 2009. Modeling and computational fluid dynamics-population balance equation-micromixing simulation of impinging jet crystallizers. Cryst. Growth Des. 9, 156–164.
Woo, X.Y., Tan, R.B.H., Chow, P.S., Braatz, R.D., 2006. Simulation of mixing effects in antisolvent crystallization using a coupled CFD-PDF-PBE approach. Cryst. Growth Des. 6, 1291–1303.
Xie, L., Luo, Z.H., 2017. Multiscale computational fluid dynamics-population balance model coupled system of atom transfer radical suspension polymerization in stirred tank reactors. Ind. Eng. Chem. Res. 56, 4690–4702.